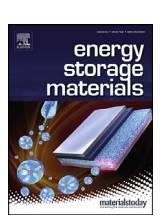
ELSEVIER

Contents lists available at ScienceDirect

# **Energy Storage Materials**

journal homepage: www.elsevier.com/locate/ensm



# Self-Stabilized $\text{LiNi}_{0.8}\text{Mn}_{0.1}\text{Co}_{0.1}\text{O}_2$ in thiophosphate-based all-solid-state batteries through extra LiOH



Yubin Zhang <sup>a,#</sup>, Xiao Sun <sup>b,#</sup>, Daxian Cao <sup>b</sup>, Guanhui Gao <sup>c</sup>, Zhenzhen Yang <sup>d</sup>, Hongli Zhu <sup>b,\*</sup>, Yan Wang <sup>a,\*</sup>

- <sup>a</sup> Department of Mechanical Engineering, Worcester Polytechnic Institute, Worcester, MA 01609, United States
- b Department of Mechanical and Industrial Engineering, Northeastern University, 360 Huntington Avenue, Boston, Massachusetts 02115, United States
- <sup>c</sup> Department of Materials Science and Nano-Engineering, Rice University, 6100 Main St, Houston, TX 77005, United States
- d Chemical Sciences and Engineering Division, Argonne National Laboratory, Lemont, IL, 60439, United States

#### ARTICLE INFO

# Keywords: Nickle-rich cathode material Self-stabilization All-solid-state batteries Interface engineering Cycle life

#### ABSTRACT

Nickle-rich LiNi $_{0.8}$ Co $_{0.1}$ Mn $_{0.1}$ O $_{2}$  (NMC 811) cathode material exhibits engaging properties in high energy density and low cost, making it great potential for the next generation high-energy all-solid-state lithium batteries (ASSLBs). However, NMC 811 suffers from severe surface electrochemical, chemical, and voltage incompatibility towards solid-state electrolytes (SSE), especially thiophosphate-based electrolytes like Li $_{6}$ PS $_{5}$ Cl. Although diverse coating methods have been made to overcome this issue, they are typically cumbersome and expensive. A coating strategy that satisfied all the requirements of cost-efficiency, stability, uniformity, scalability, and easy-achieving is still challenging. In this work, we developed a LiOH-based surface stabilization strategy that provides a ~10 nm stable permeable layer on NMC 811. After one-step sintering of NMC 811 precursor mixed with LiOH, which is commonly used for NMC 811 lithiation process, excessive LiOH simultaneously distributes on NMC 811 particles. Unlike other reported methods, this coating method can be easily controlled and fabricated without additional complicated processes. By simply controlling the thickness of LiOH layer, which protects the Li $_{6}$ PS $_{5}$ Cl solid electrolyte materials from being oxidized, optimized cycling stability can be obtained for 600 cycles with capacity of 130 mAh g $^{-1}$ 0 on average at a wide electrochemical window of 2.50–4.20 V (vs. Li-In).

#### 1. Introduction

All-solid-state Li-ion batteries (ASSLBs) are attracting much attention due to the satisfaction of high safety, excellent electrochemical cycling property and long-term stability. To date, various solid electrolytes, including oxide, sulfide, and polymer and composite electrolytes, have been developed for ASSLBs. Sulfide solid electrolyte is one of the most promising candidates for ASSLBs due to their ultrahigh ionic conductivity (>10 $^{-3}$  S cm $^{-1}$ ) at room temperature. Meanwhile, sulfide electrolytes are featured with soft property, which enables facile processing, like cold pressing, and intimate interface contact with electrodes. [1] Among various choices, Li<sub>6</sub>PS<sub>5</sub>Cl gains wide attention because it exhibits high ionic conductivity ( $\sim 2\times 10^{-3}$  S cm $^{-1}$ ), low cost, and facile synthesis.

For the different cathode materials in rechargeable lithium-based batteries, layered lithium transition metal oxides (TMO) with  $\alpha$ -NaFeO<sub>2</sub>

crystal structure have received the most attention in the past decades. Conventional LiCoO<sub>2</sub> (LCO) cathode, originally commercialized by Sony in the 1990s, has been widely used in electronics, such as cell phones, cameras, and laptops. [2] However, the high cost [3] prevented its practical application in automotive industry. In contrast, Ni and Mn metals are abundant on earth. Consequently, significant research efforts have been devoted to the development of TMO intercalation materials containing little or no Co in the last few years. In particular,  $\text{Li}(\text{Ni}_x \text{Mn}_y \text{Co}_z) \text{O}_2 \ (x+y+z=1, \text{NMC})$  is predominant due to their outstanding stability as well as lower cost compared with  $\text{LiCoO}_2$ . [4–7] In addition, high nickel  $\text{LiNi}_{0.8} \text{Co}_{0.1} \text{Mn}_{0.1} \text{O}_2$  (NMC 811) is regarded as one of the most advanced material choices in future electric vehicle technology because of their higher lithium utilization rate (discharge capacity exceeding 200 mAh g  $^{-1}$ ) [8] and relatively high average operating voltage (3.6 V vs.  $\text{Li/Li}^+$ ) [9].

To satisfy the requirements of energy density and safety of batteries, it is appealing to apply NMC 811 with  $\rm Li_6PS_5Cl$  in ASSLBs. However, the sulfide electrolyte is electrochemically and chemically unsta-

<sup>\*</sup> Corresponding author.

E-mail addresses: h.zhu@neu.edu (H. Zhu), yanwang@wpi.edu (Y. Wang).

<sup>&</sup>lt;sup>#</sup> Y. Z. and X. S. contributed equally to this work.

ble with many state-of-the-art cathode materials, especially under high voltage, such as  ${\rm LiCoO_2},\,{\rm LiNi_{1/3}Co_{1/3}Mn_{1/3}O_2},\,{\rm and}\,\,{\rm LiMn_2O_4}$  [10]. To overcome the interfacial issue, coating is one of the most common and efficient methods, which could not only avoid side reactions between the highly reactive Ni<sup>4+</sup> and Li<sub>6</sub>PS<sub>5</sub>Cl electrolyte, where Li<sub>6</sub>PS<sub>5</sub>Cl could be oxidized into poor ionic and electronic conductive products, such as Li polysulfide and sulfur, [11] but also serve as a physical barrier of the cathode material to minimize phase change and improve structural stability. [12] Several coating materials have been investigated, and the preferred option is to incorporate compounds containing lithium as the coating film, such as Li<sub>0.35</sub>La<sub>0.5</sub>Sr<sub>0.05</sub>TiO<sub>3</sub> through sol-gel method. [11] Coating materials with higher conductivities are also investigated, such as  $\text{Li}_3 \text{VO}_4$  (1.24×10<sup>-4</sup> S cm<sup>-1</sup>), [13]  $\text{Li}_2 \text{ZrO}_3$  (3.3 × 10<sup>-5</sup> S cm<sup>-1</sup>) [14], and LiNbO<sub>3</sub> ( $10^{-5}$  S cm<sup>-1</sup>) [15] surface coatings on nickel-rich layered oxide cathode. However, the sol-gel coating method depends on particle morphology and structure stability, which might reduce the capability of applications with other cathode materials, and the complex preparation limits their further applicability in mass production.

Conventional methods to produce the coating can be divided into several categories: atomic layer deposition (ALD), chemical vapor deposition (CVD), wet chemical methods, and dry-mixing methods. ALD is known for its ability to deposit conformal films with atomic thickness, and has been successfully used to form different coatings, such as  $LiAlF_4$ , [16]  $Al_2O_3$ , [4]  $Al_2O_3$ - $Ga_2O_3$ , [17] and ZnO [18] on NMC. However, ALD requires specialized equipment and multiple steps, so is the CVD coating method. [19] Both wet chemical methods and dry methods have also been extensively investigated. Sol-gel coating is one of the thoroughly utilized wet chemical methods and has been used for depositing  $Al_2O_3$ , [20]  $TiO_2$ , [21] and  $Li_{3x}La_{2/3-x}TiO_3$  [11] coating successfully. These wet chemical methods typically result in thicker and more irregular layers. Dry coatings tend to be ununiform and inconsistent. [22] It should be stressed that the consistency and efficiency of NMC coating largely depend on the process and conditions of the coating process and NMC's physical properties such as surface area.

Although many efforts have been made to develop coatings for cathode materials in order to be used in ASSLBs, there is still a lack of a coating method protecting the interface while remain cost-efficient, scalable, and simple to achieve. In this work, we developed a one-step process, and LiOH-coated-LiNi $_{0.8}$ Co $_{0.1}$ Mn $_{0.1}$ O $_{2}$  (LiOH–NMC 811) cathode material can be synthesized directly from the precursor without any subsequent treatments. This work allows the precursor to undergo lithiation as extra LiOH forms a coating on the cathode powder simultaneously, which dramatically improves cathode preparation efficiency and will lower the cost of mass production significantly. The 10% LiOH–NMC 811 has an exceptional specific capacity of 130 mAh g $^{-1}$  on average with an ultra-stable 600 cycles with columbic efficiency of 98% and 90% capacity retention. The method provides a new solution to stabilize the cathode interface through a low-cost and scalable process to enable high-performance ASSLBs.

## 2. Experimental

#### 2.1. Precursor preparation

Nickel sulfate hexahydrate (GFS Chemicals (Columbus, OH)), manganese sulfate monohydrate (GFS Chemicals (Columbus, OH)) and cobalt sulfate (GFS Chemicals (Columbus, OH)) were dissolved at a molar ratio of 8:1:1 in de-ionized water. Then metal sulfate solution (Ni / Mn / Co), ammonia solution (32%, EMD Millipore), and sodium hydroxide (VWR) were fed into a continuous stirred tank reactor (CSTR) under nitrogen. During the entire reaction, the process parameters like pH, flow rate, and temperature were controlled based on our previous work. [23] After co-precipitation reaction, the suspension was filtered and thoroughly washed at the end of the experiment to remove residual or absorbed salts. The precursor powders (  $[\mathrm{Ni}_{0.8}\mathrm{Mn}_{0.1}\mathrm{Co}_{0.1}](\mathrm{OH})_2)$  were then dried overnight in an oven at 130 °C.

#### 2.2. Cathode sintering

Precursor particles at different time were collected for cathode sintering to form uniform size distribution and moderate flake thickness. In order to synthesize the cathode active material, 1 mol of the precursor (  $[{\rm Ni}_{0.8}{\rm Mn}_{0.1}{\rm Co}_{0.1}]({\rm OH})_2)$  was mixed with (1 + x) mol of LiOH•H<sub>2</sub>O (x = 5%, 7.5%, 10%, 12.5% and 15%) (VWR), which was marked as x LiOH–NMC 811. The mixture was firstly sintered at 450 °C for 5 hrs, followed by another 15 hrs at 775 °C. Both heating and cooling rates were 2 °C/min in each step. The sintering was done in a tube furnace flowed with pure oxygen. After cooling down to room temperature, the cathode powder was grounded to ensure that the material did not contain any agglomerates.

#### 2.3. The soluble base content (SBC) test

The Soluble Base Content (SBC) Test was conducted with Accumet-Comm software connecting to a pH electrode. The pH electrode was firstly calibrated with standard solutions of 4.0 and 7.0 at room temperature. The calibrated slope should be greater than 99.0%. 5 g of assintered cathode powder was transferred from oxygen-filled tube furnace directly to avoid further air exposure. Then 100 g of de-ionized (DI) water was added in a closed flask and stirred for 10 min. The slurry was then filtered immediately and about 98–99 g of clear solution was obtained. 90 g of the clear solution was taken for the pH titration experiment and can be kept in an open 250 ml glass flask. During the pH titration experiment, the electrode was inserted into the clear solution with continuous stirring. The addition of acid (0.1 M HCl, Sigma-Aldrich) was started in 30 s. The acid was added at a rate of 0.5 ml/min. pH data points were recorded every 3 s until a value below pH-3.0 was achieved.

Only two contributions are considered to be present in the whole base: (1) LiOH and (2) Li $_2$ CO $_3$ . Two inflection points can be seen in a normal pH titration. The first is at a pH of 8.4, while the second is at a pH of 4.7, approximately. Both inflection points are Li $_2$ CO $_3$  type bases, and they can be used to calculate the amount of Li $_2$ CO $_3$  type base. The Li $_2$ CO $_3$  value is deducted from the total base to obtain the LiOH type base. The values are corrected for the sample mass and the percentages of solution used in the pH titration experiment to yield the "weight-specific soluble base content" (per g of cathode). The results can be expressed in terms of wt.% of LiOH or wt.% of Li $_2$ CO $_3$ , which goes back to the concept of soluble base as "impurity."

The SBC values can be calculated by [24]:

$$SBC - Li2CO3 \text{ (wt\%)} = \frac{(V2 - V1) \times C_{HCl} \times M_{Li2CO3}}{1000 \times \left\{ \left( W_{LMO2} \times W_{solution} \right) \middle/ W_{DIwater} \right\}} \times 100(\%)$$

$$SBC - LiOH (wt\%) = \frac{(2 \times V1 - V2) \times C_{HCI} \times M_{LiOH}}{1000 \times \left\{ \left( W_{LMO2} \times W_{solution} \right) / W_{DIwater} \right\}} \times 100(\%)$$

wherein:

V1,V2: ml of acid at inflection point 1, 2 (V2 > V1);

C. concentration of HCl (0.1 mol/L);

W: weights of sample LiMO, used solution and stirred water;

M: molecular weights.

#### 2.4. Structure characterization

Scanning Electron Microscope (SEM) images of the particles was obtained with JEOL JSM 7000 F at 5 kV operating voltage for the precursor and 10 kV for the cathode with an energy-dispersive X-ray spectroscopy (EDS) detector. PANalytical Empyrean was used with the Cu K $\alpha$  source ( $\lambda=1.54178$  Å) to conduct X-ray diffraction (XRD) and data was obtained with a step size of 0.03° and a spinning dwell time of 60 s. Rietveld refinement results are obtained by FullProf software.

High-angle annular dark-field scanning transmission electron microscopy (HAADF-STEM) images were obtained at the Electron Microscopy Center (EMC) of Rice University. The samples were prepared

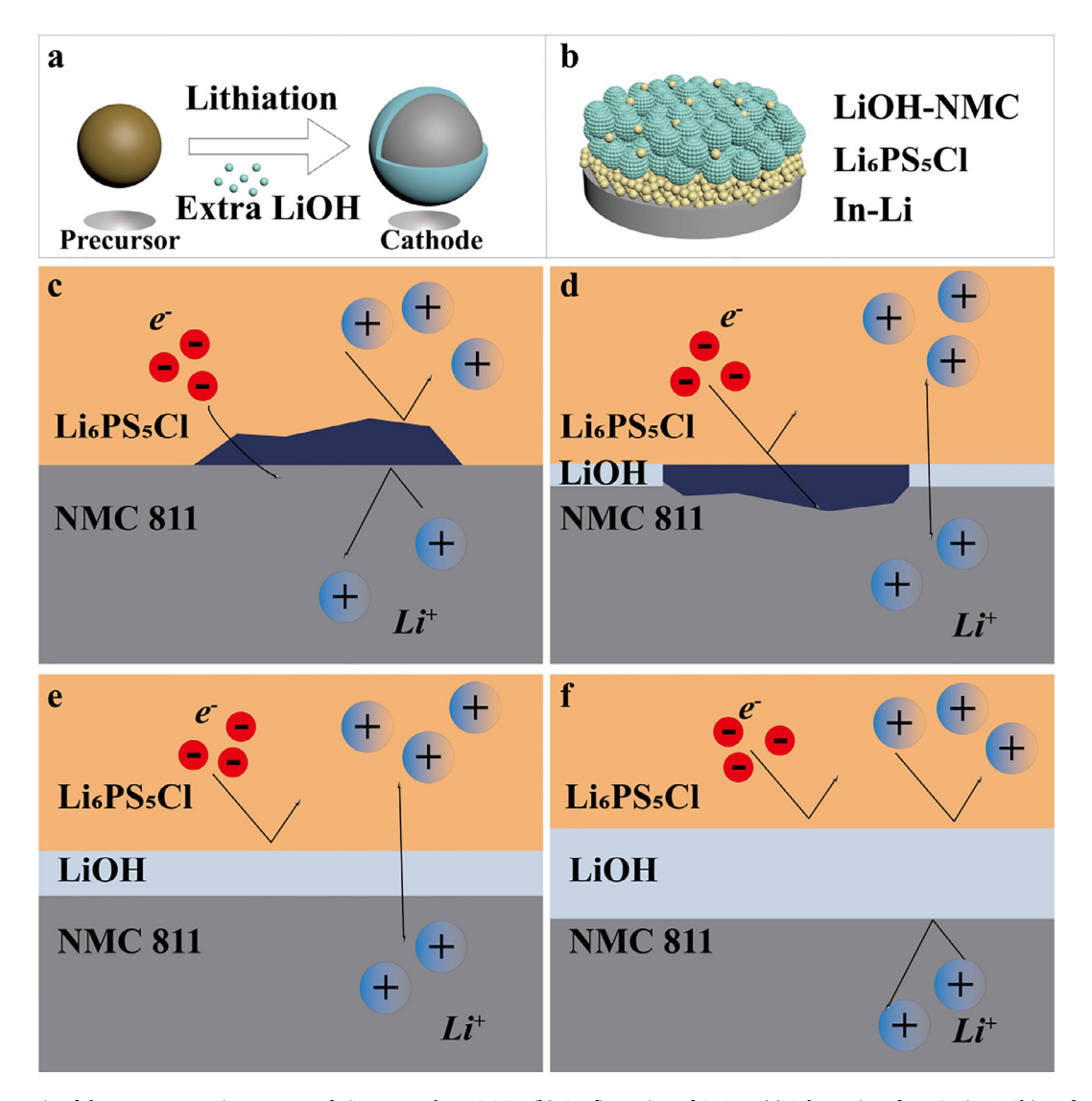


Fig. 1. (a) Schematics of the one-step coating process of LiOH coated NMC 811; (b) Configuration of ASSLB; (c) Schematics of NMC/Li<sub>6</sub>PS<sub>5</sub>Cl interfacial incapability without coating; (d) Schematics of NMC/Li<sub>6</sub>PS<sub>5</sub>Cl interface with optimized coating; (f) Schematics of NMC/Li<sub>6</sub>PS<sub>5</sub>Cl interface with optimized coating; (f) Schematics of NMC/Li<sub>6</sub>PS<sub>5</sub>Cl interface with superfluous coating.

with Focused Ion Beam (FIB, ThermoFisher Helios Nanolab 660) at  $30\ kV$  and polished at  $5\ kV$  for cross-section view, subsequently.

X-ray photoelectron spectroscopy (XPS) data for NMC 811 samples including both pristine and particles coated with LiOH were acquired using PHI 5000 VersaProbe II system (Physical Electronics). The X-ray source was operating at 25 W equipped with monochromatic Al K $\alpha$  radiation (hv = 1486.6 eV) which was set at Ar<sup>+</sup>-ion and electron beam sample neutralization, fixed analyzer transmission mode. The base pressure in the XPS chamber was  $\sim 1 \times 10^{-8}$  torr. The spectra of all samples were collected at a pass energy of 23.50 eV and electron escape angle of 45° to the sample plane. The spot size for X-ray beam was set to be 100  $\mu$ m. The spectrum was calibrated against C–C at 284.8 eV. The Shirly background data were subjected from all spectra. The spectra were fitted to multiple Gaussian-Lorentz peaks by using the software package (Multipack) that Physical Electronics provided.

#### 2.5. Fabrication of ASSLBs

The fabrication of all-solid-state lithium batteries (ASSLBs) was conducted in a glovebox with oxygen and water amounts lower than 0.05 ppm. NMC 811 powder which was coated with different amount of LiOH (5%, 7.5%, 10%, 12.5%, and 15%) were manually mixed with

 ${\rm Li_6PS_5Cl}$  powder at a weight ratio of 70:30 to make the cathodes. In a homemade pressurized cell, 200 mg of  ${\rm Li_6PS_5Cl}$  was first pressed into a pellet with a diameter of 12.7 mm under a pressure of 100 MPa. Then, 10 mg of prepared cathode powder was cast onto one side of the pellet, and In-Li foil was placed on the other side. A piece of Cu foil and Al foil are selected as the current collector for anode and cathode, respectively. After the subsequent pressing under a pressure of 300 MPa, the ASSLBs with a sandwiched structure were assembled. An extra pressure of 50 MPa was applied during measurement.

### 2.6. Electrochemical characterization of ASSLBs

All the ASSLBs are tested with an electrochemical station (Biologic SP150) at room temperature. The rate and cycling performance were measured with galvanostatic cycling with potential limitation protocol between the cutoff voltages of 2.5 and 4.2 V (vs. Li-In). The current was based on the area of SSE pellet (12.7 mm in diameter). The cyclic voltammetry (CV) was carried in the range of 2.5–4.2 V (vs. Li-In) at a scan rate of 0.1 mV/s. Electrochemical impedance spectroscopy (EIS) was conducted with an amplitude of 10 mV in the frequency range of 1 MHz to 10 mHz.

#### 2.7. Electrochemical testing in liquid electrolyte

Cathode powder (x% LiOH-NMC 811), conductive carbon (super C65), and dissolved polyvinylidene fluoride (PVDF) in N-Methyl-2pyrrolidone (NMP) were uniformly mixed. The slurry was then cast onto an aluminum foil and then dried for 8 hrs. at 60 °C. Electrode discs with a diameter of 12 mm were punched and pressed to achieve the desired porosity before assembly into the coin cells. Any excess solvent was evaporated after being dried in the vacuum oven for 8 hrs. A polypropylene-polyethylene-polypropylene (MTI Corporation) tri-layer membrane with 25 µm was chosen as the separator. Liquid electrolyte consisted of an ethylene carbonate (EC)/Ethyl Methyl Carbonate (EMC) composition (3:7 wt ratio) with 1.0 M LiPF<sub>6</sub>. Electrochemical performance tests were performed with an Arbin (Model BT2043) instrument. The first two cycles were usually measured with a current density of C/10 (1 C = 200 mA/g), followed by C/2 for the subsequent cycles. Furthermore, the rate performance was checked at different C rates (C/10, C/5, C/2, C, 2C, 3C, 5C and 10C), where both the charge and discharge rates were varied.

#### 3. Results and discussion

A schematic diagram of the one-step coating process is shown in Fig. 1a, in which the precursor (  $[\mathrm{Ni}_{0.8}\,\mathrm{Mn}_{0.1}\mathrm{Co}_{0.1}](\mathrm{OH})_2)$  is firstly combined with an additional amount of LiOH. The excess LiOH+H<sub>2</sub>O played two roles in this step: (1) it compensated for the loss of lithium during the calcination process; (2) the residue lithium formed a coating layer on the NMC particles at the same time. Compared to other reported methods, such as ALD, CVD, wet-chemistry and dry-mixing methods, this one-step method shows great advantages in simplifying the procedure: it does not involve any complex preparation; moreover, it has no requirement of the equipment or coating materials, which saves plenty of costs and is appliable to various cathode system. The comparison of different coating processes is shown in Table S1.

**Fig. 1b** demonstrates the configuration of ASSLBs assembled with LiOH coated NMC 811 as cathode, where Li<sub>6</sub>PS<sub>5</sub>Cl was mixed to ensure the Li-ion transfer. Li-In was used as anode to avoid the interface reaction between Li and Li<sub>6</sub>PS<sub>5</sub>Cl. **Figs. 1c-f** illustrate the mechanism of LiOH coating at the interface between NMC 811 and Li<sub>6</sub>PS<sub>5</sub>Cl. As shown in **Fig. 1c**, Li<sub>6</sub>PS<sub>5</sub>Cl can be oxidized by NMC 811 at physical contact without interfacial engineering, and this reaction will be fur-

ther accelerated at an elevated potential. [11] The side products, such as Li polysulfide and sulfur at the interface, come with poor electronic and ionic conductivities, although prevent  $\mathrm{Li}_6\mathrm{PS}_5\mathrm{Cl}$  from further degradation, they greatly impede the diffusion of  $\mathrm{Li}^+$  and leads to loss of capacity and lower energy density. [11]

When only a low amount of extra LiOH was applied, as shown in Fig. 1d, the thin LiOH coating layer incompletely covered on the interface. At the interfacial area where LiOH is not sufficiently covered, the oxidation reaction is only partially impeded. In another words, Li<sub>6</sub>PS<sub>5</sub>Cl can still in contact with NMC directly, this could lead to irreversible side reactions at the interface, and generate passivated products, and a significant increase of interfacial resistance. As more LiOH applied, the coating should be thicker and ensure a more comprehensive coverage on NMC 811 particles, when the coating achieves a balance that enable Li-ion diffusion and fully coverage as a protective barrier to avoid physical contact, as shown in Fig. 1e, the optimization condition occurs. At this circumstances, since Li<sub>6</sub>PS<sub>5</sub>Cl is soft and deformable in pressurized condition, LiOH coating can fully cover the interfacial area between NMC 811 and Li<sub>6</sub>PS<sub>5</sub>Cl. The LiOH layer, herein, allows Li-ion diffusion while preventing electrons transfer, thus, protects Li<sub>6</sub>PS<sub>5</sub>Cl from side reactions. It should also be mentioned that LiOH coating layer will not affect the electrons pathway among NMC particles. In the cathode electrode layer, coated NMC 811 particles will also be pressed, which will cause fracture of LiOH coating at NMC/NMC interface ensured by rigid mechanical property of NMC particles. This makes it possible to allow electrons transfer among NMC particles, and ensure the electrochemical intercalation/deintercalation reactions. When the LiOH coating layer is superfluous, like in Fig. 1f, even though electron transfer is almost completely prevented between NMC 811 and Li<sub>6</sub>PS<sub>5</sub>Cl, the diffusion of Li<sup>+</sup> is also greatly limited. Thus, electrochemical reaction can be suppressed, resulting in a high capacity lose and low Coulombic efficiency. To study the effect of the thickness of the coating, we developed a process starting with the precursor of NMC 811. Precursors were synthesized through the co-precipitation reaction, which is similar to our previous work. [22]

Figs. 2a-e compares NMC 811 precursor morphology that formed during different time interval. Particles from 3 to 6 h. (Fig. 2a) have an irregular morphology with thin flakes. The secondary particles become larger and more spherical due to the insertion of primary particles with continuous reaction progresses, as shown in Fig. 2b, where flakes often grow to be thicker as well. The large particles no longer grow much after 18 h. (Fig. 2c) due to the kinetic equilibrium of insertion and crystal-

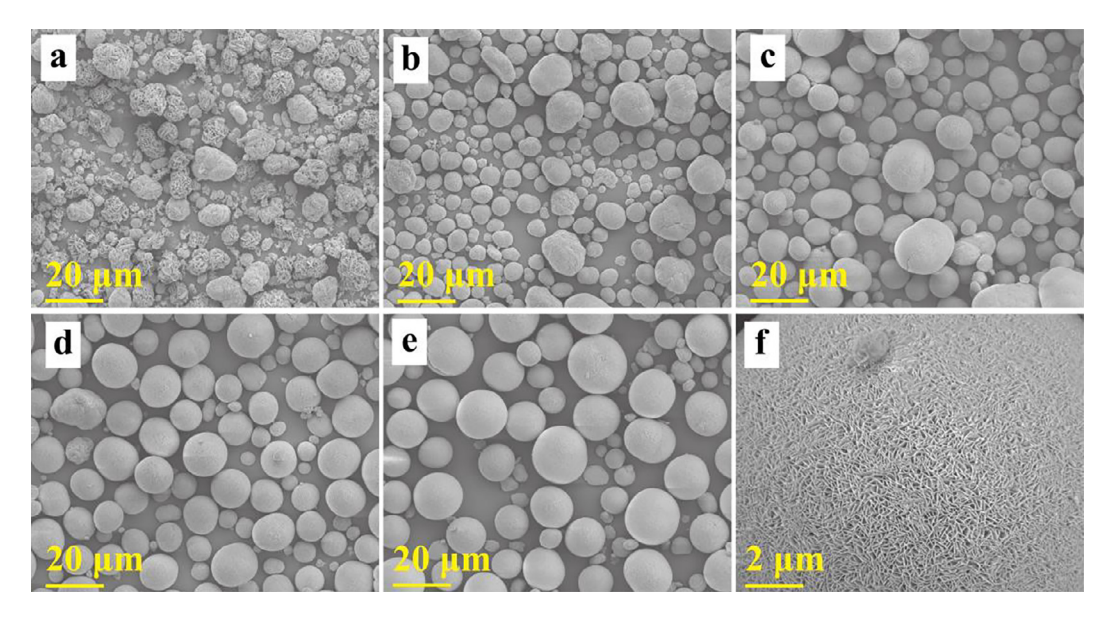


Fig. 2. (a-e) SEM of precursors obtained from: (a) 3–6 h; (b) 9–12 h; (c) 15–18 h; (d) 21–24 hrs; (e) 27–30 h.); (f) Zoom-in figure of the surface morphologies for precursor particles from 21 to 24 h.

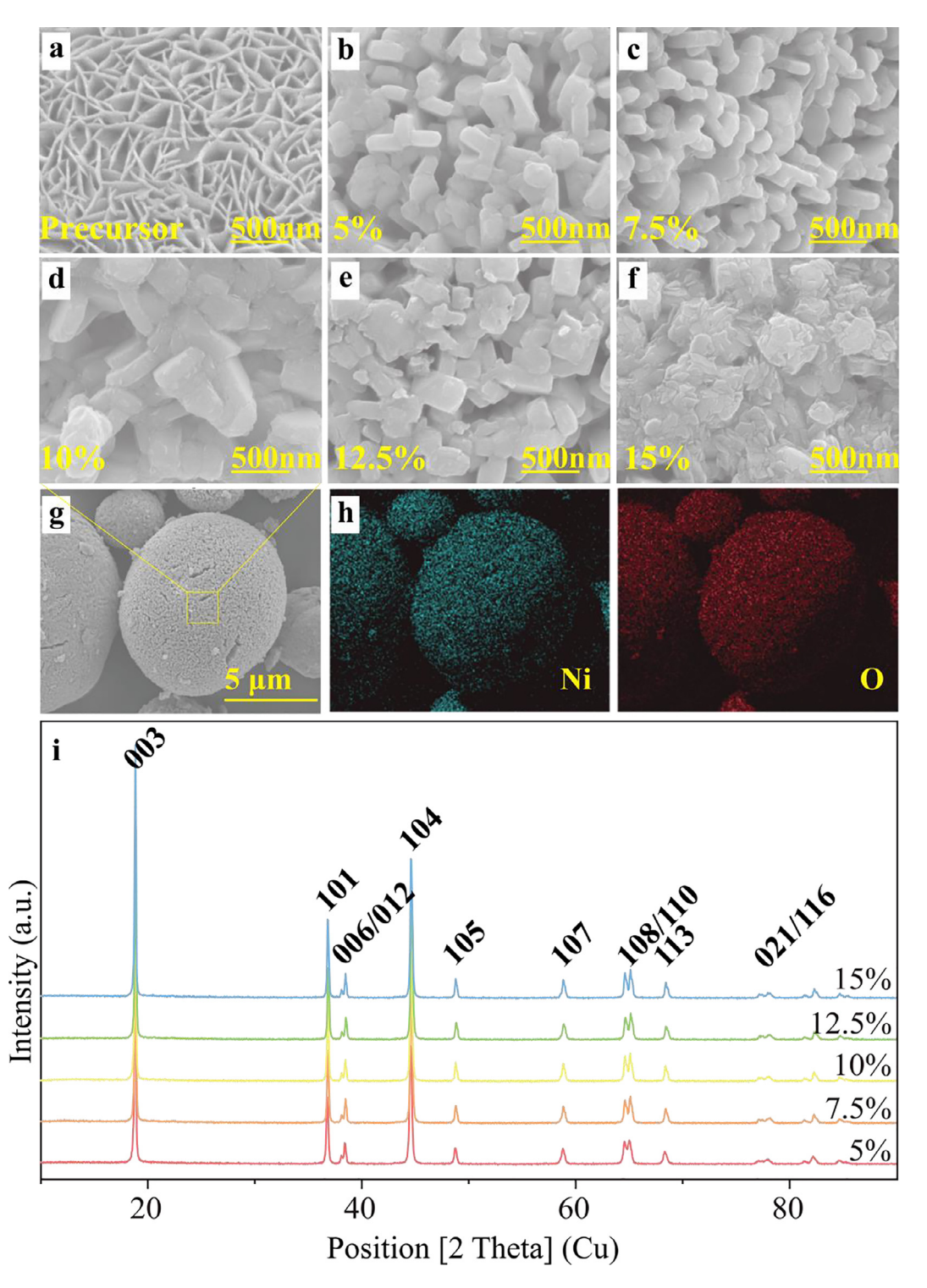


Fig. 3. SEM of NMC 811 precursor and cathodes sintered with various amount of extra LiOH: (a) precursor from 21 to 24 h.; (b) 5%; (c) 7.5%; (d)10%; (e) 12.5%; (f) 15%; (g) SEM images of 10%ex LiOH–NMC 811; (h) EDS mappings for Ni and O elements; (i) XRD patterns of 5–15% ex LiOH–NMC 811 s.

lization in the reaction system. This kind of spherical morphology helps achieve high density for NMC cathode material in application. Comparing Fig. 2d and 2e, after 24 h the number of irregular shaped small particles is increased, which is not favorable for surface modification. Among them, the precursor displays tens of micron-sized spherically shaped particles at 21–24 h (Fig. 2d) with a nearly uniform size distribution ( $d=12~\mu m$  approximately) and uniform surface morphology (Fig. 2f), which are chosen for surface coating.

The XRD analysis was conducted on the precursor of 21–24 h. Sample, shown in **Figure S1**. The spectra of  $[Ni_{0.8}Mn_{0.1}Co_{0.1}](OH)_2$  compound is similar to the spectra of pure  $\beta$ -Ni(OH)<sub>2</sub>. [25] All diffraction lines are indexed to a hexagonal structure with a space group of P $\bar{3}$ m1.

Thus, precursor powder from 21 to 24 h. (Fig. 3a) was used to achieve a uniform coating. At a molar ratio of 1: (1 + x) (where x = 5%, 7.5%, 10%, 12.5%, 15%), the precursor was combined with LiOH salts. To compensate lithium loss during sintering, extra 5% of LiOH was

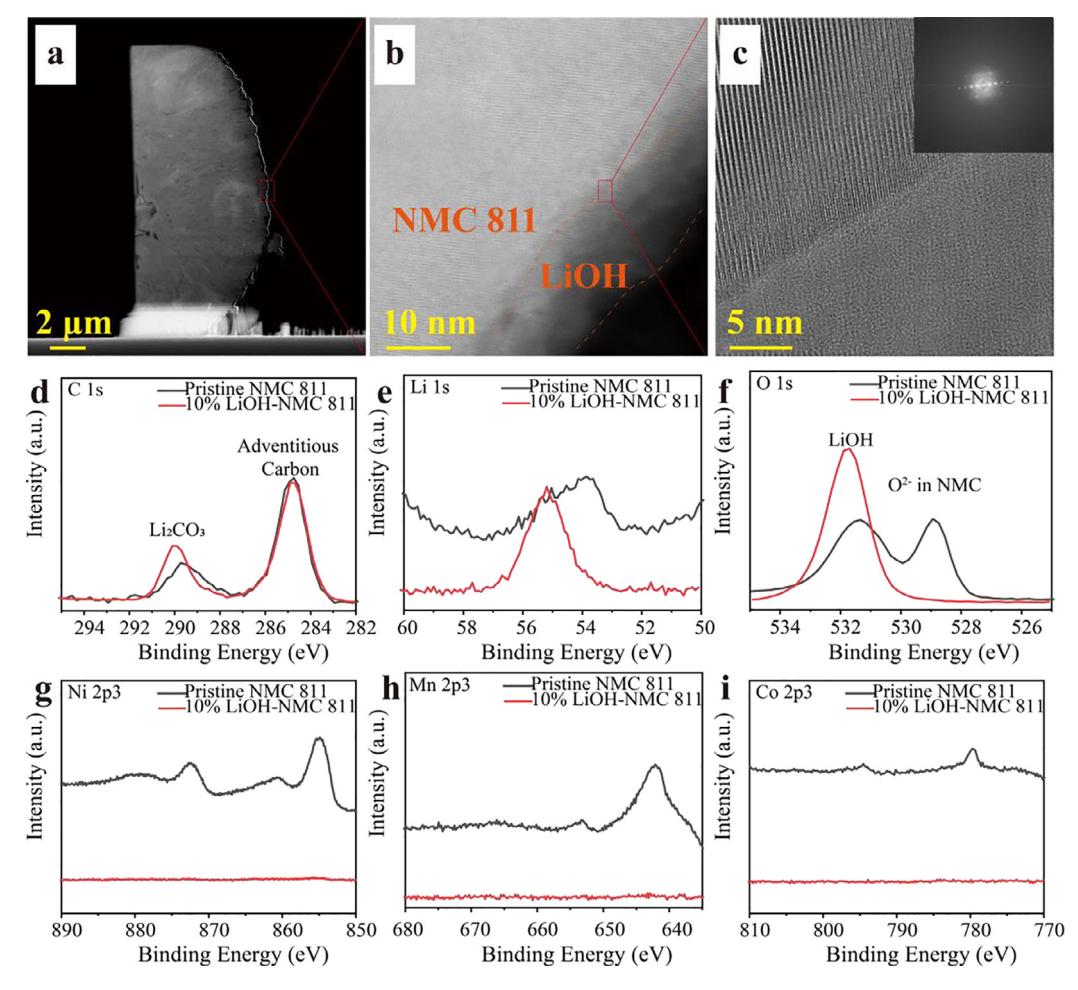


Fig. 4. Cross-section STEM images of 10% LiOH–NMC 811 particle and XPS spectra of 10% LiOH–NMC 811 compare with pristine NMC 811. (a) Cross-section HAADF-STEM image of 10% LiOH–NMC 811; (b) and (c). HAADF images (at different scale), inset shows the corresponding FFT pattern of NMC layered structures; (d-i) XPS spectra of the pristine and 10% LiOH–NMC 811: (d) C 1 s, (e) Li 1 s, (f) O 1 s, (g) Ni 2p3, (h) Mn 2p3 and (i) Co 2p3.

added as to synthesis the pristine NMC 811. SEM images of NMC 811 cathodes with x excess LiOH are shown in Figs. 3b-f, and it can be clearly observed that the spherical morphology of particles was maintained even after the thermal treatment process, whereas major variations can be observed between the surface morphology of particles with different x LiOH. There is no apparent coating structure formed on the secondary particles of NMC 811 at points where x is less than 10%; with additional LiOH applied, those primary particles were gradually covered by a layer of secondary phase structure formed from excess LiOH; when x is greater than 10%, the secondary particles of NMC 811 were completely covered with LiOH.

The accurate amount of LiOH in each cathode material was calculated based on the sum of the soluble base content (SBC) results listed in **Table S2**. Since LiOH is chemically unstable in air or water, LiOH was partially converted into  ${\rm Li}_2{\rm CO}_3$  during measurement. However, it was still reasonable to assume the original amount of LiOH base on the concentration of  ${\rm Li}^+$  (LiOH and  ${\rm Li}_2{\rm CO}_3$ ) in total.

**Fig. 3g** shows the surface morphology of 10% LiOH coated NMC 811 particles at lower magnification. From the figure, it can be observed that the particle possesses a smooth and uniform surface morphology. This coating layer was generated onto the NMC 811 particles simultaneously during cathode sintering process. The anticipated homogeneous distribution of characteristic transition metals Ni and O are observed from the EDS mapping results shown in **Fig. 3h**. All elements detected are distributed homogeneously on the particles and no other impurities have been detected.

The XRD patterns of LiOH-coated NMC 811 materials are shown in Figs. 3i. All diffraction peaks could be indexed to the hexagonal NaFeO<sub>2</sub> structure with the  $R^3$ m space group in which the 3a, 3b, and 6c octahedral sites are occupied by Li, TM, and oxygen atoms. No other phase containing crystalline Li was found for the coated samples. Fig. S2 shows the XRD refinement results of x% LiOH–NMC 811 and Table S3 lists the refined lattice parameters of the samples. For each of them, the Chi² is 2.95, 2.80, 3.57, 3.75, and 2.83, demonstrating the excellent fit and accurate structural data collected. The unit cell volumes did not change much compared to the pristine NMC 811 (5% LiOH–NMC 811). Therefore, LiOH coating shows no negative effects on crystal structure of NMC 811 cathode particles. Furthermore, the identical c/a values (4.9472, 4.9505, 4.9501, 4.9530, and 4.9532 are all about 4.95) and the simple splitting of the diffraction peaks (108)/(110) for all samples (Fig. 3c) indicate the formation of a well-ordered layered structure.

The interface of the active material particle was examined by cross-section STEM to further confirm the presence of the coating layer at the surface of the modified NMC 811 sample. Fig. 4a describes the cross-section view of 10% LiOH–NMC 811 particle with STEM characteristics. The technique of FIB was used for cutting the 10% LiOH–NMC 811 particle and polishing to obtain a better view of the cross-section, followed by measuring internal morphology and distribution of components. As shown in the HAADF-STEM images Fig. 4b, the tightly packed particle is covered by a uniform nanosized LiOH coating layer, with a thickness of 10 nm approximately. Fig. 4c shows the interphase grain boundary between NMC 811 and LiOH. There is no separation observed, which

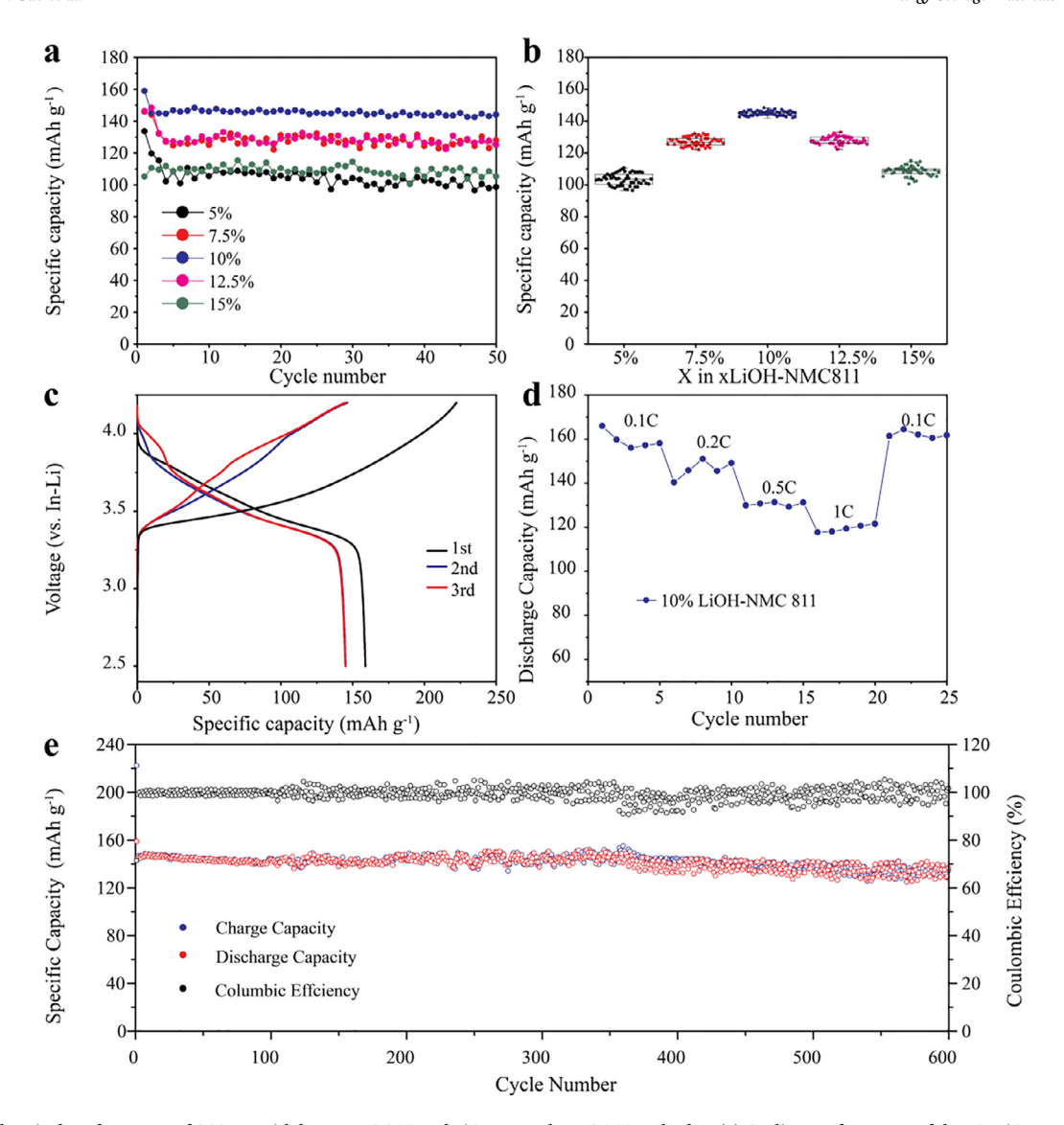


**Fig. 5.** Electrochemical performance of ASSLBs with bare NMC 811 and LiOH coated NMC 811 cathodes. (a) Cycling performance of the x% LiOH–NMC 811 electrode at 0.126 mA cm<sup>-2</sup> (0.1C); (b) Discharge capacity distribution at different LiOH coating ratios; (c) The galvanostatic charge–discharge voltage profiles of the 10% LiOH–NMC 811 electrode between 2.5 and 4.2 V (vs. Li-In) at a current density of 0.126 mA cm<sup>-2</sup>; (d) Rate performance at current densities ranging from 0.126 to 1.26 mA cm<sup>-2</sup>; (e) Long-cycling performance of ASSLB with 10% LiOH–NMC 811 at 0.1C.

further confirmed the coating was successfully generated onto NMC 811 particles.

In order to investigate the existence of LiOH coating on NMC 811, the X-ray photoelectron spectroscopy (XPS) spectra for both pristine and 10% LiOH–NMC 811 are displayed in **Figs. 4d-i**, respectively. In the C 1 s XPS spectra (**Fig. 4d**), peak at 285 eV corresponds to adventitious carbon from the internal calibrator, the other peak at 290 eV is originated from Li<sub>2</sub>CO<sub>3</sub>. [26] After the normalization of the peak intensities of the adventitious carbon, 10% LiOH–NMC 811 displays a slightly higher amounts of the residual Li<sub>2</sub>CO<sub>3</sub>. The higher concentration of Li<sub>2</sub>CO<sub>3</sub> on LiOH–NMC is reasonable due to the extra amount LiOH coated outside of NMC particle surface, and since the eventual contact with air during testing, LiOH can turn into Li<sub>2</sub>CO<sub>3</sub> easily, which further increase the amount of Li<sub>2</sub>CO<sub>3</sub> on the surface of LiOH–NMC particles.

Of the Li 1 s spectra (Fig. 4e), 10% LiOH–NMC 811 reveals a relative much larger concentration of Li than that of the pristine NMC 811 due to the existence of LiOH coating, thinking of the approximate concentration of Li<sub>2</sub>CO<sub>3</sub>, this could be an evidence proving the composition of coating is LiOH mainly. The O 1 s spectra (Fig. 4f) also consist of

two peaks, corresponding to the LiOH peak at 532 eV from the surface coating layer and the  ${\rm O^{2-}}$  ion peak at 528 eV in NMC 811 particles inside. [27] The corresponding peak located at 532 eV is in accordance with LiOH, and the higher intensity identifies the composition as LiOH. The peak for Li<sub>2</sub>O should be at 530 eV, which is not detected. Thus, we conclude the coating layer is LiOH rather than Li<sub>2</sub>O. By comparison, signals of  ${\rm O^{2-}}$ , Ni, Mn and Co from NMC 811 were not observed in the LiOH–NMC particles(Figs. 4f-i), this can be addressed by the coating fully covered the NMC particle surface and no TM signals could be captured. It also confirmed the NMC particles were fully covered by LiOH coating, and the composition of the coating layer can therefore be described as LiOH.

The electrochemical performance of x LiOH–NMC 811 s is investigated in ASSLBs to further evaluate the significance of the interface engineering. Although conductive carbon increases the electronic conductivity of the cathode, it significantly improves the oxidation of  $\text{Li}_6PS_5Cl$  at high voltage (>3 V). Therefore, at the interface between the  $\text{Li}_6PS_5Cl$  and carbon, a layer of decomposed products would form. These products at the interface will, to some degree, prevent further reaction. Because of their low ionic conductivity, the decomposed products would

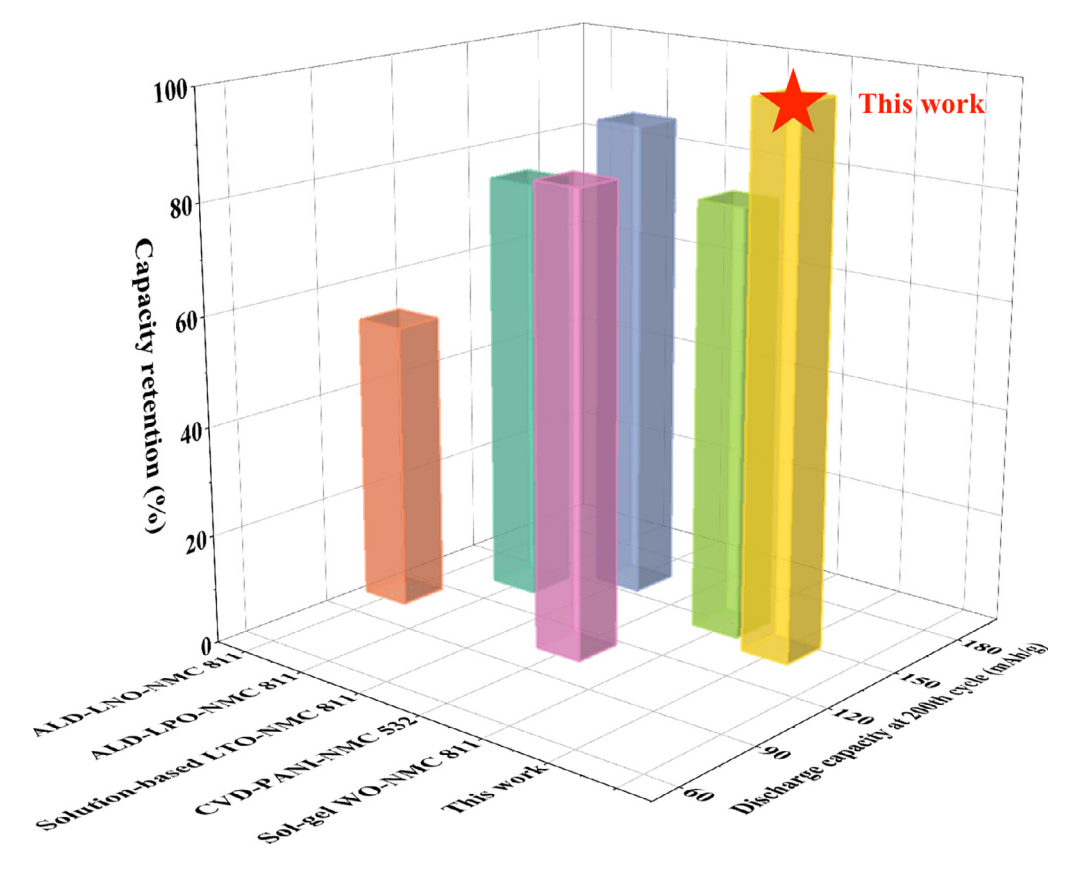


Fig. 6. Comparison of capacity retention and discharge capacity at the 200th cycle.

increase the ion transport resistance in the cathode, which will compromise the cell performance. No conductive additives are added in the cathode portion to prevent the degradation caused by carbon. Without carbon, electrons can still transfer among NMC particles. LiOH coated NMC particles will be compressed in cathode electrode layer. Due to the small thickness of LiOH layer compared to NMC particles, during the pressing process, the LiOH coating layer is hard and brittle, it will fracture at the point contact of the NMC particles, which allows electron transfer. [28] On the contrast, at the interface between NMC and  $\text{Li}_6\text{PS}_5\text{Cl}$ , thinking of the deformability of  $\text{Li}_6\text{PS}_5\text{Cl}$ , it is much easier to maintain the LiOH coating structure. Thus, the LiOH layer can play the role of protecting the interface between NMC and  $\text{Li}_6\text{PS}_5\text{Cl}$ .

To avoid the side reaction between Li<sub>6</sub>PS<sub>5</sub>Cl and Li metal, Li-In is selected as the anode. All ASSLBs tests are conducted at room temperature after being assembled. The cycling performance at a constant current density of  $0.126~\text{mA}~\text{cm}^{-2}$  (approximately 0.1C) of the x LiOH–NMC 811 was also investigated after 3 cycles of formation conducted at the current density of 0.126 mA cm<sup>-2</sup>, and the results are shown in Figs. 5a and **5b**. The 10% LiOH–NMC 811 cell delivers a capacity of 159 mAh g<sup>-1</sup> at the 1st cycle and 144 mAh g<sup>-1</sup> at the 50th cycle with 99.2% capacity retention, while the samples of x = 5%, 7.5%, 12.5% and 15% showed lower capacity and capacity retention, from 98.6 to 127.9 mAh g<sup>-1</sup> and 96.2% to 97.0% respectively. Since we did not do formation cycles initially for those cells, the capacity retentions are calculated based on the discharge capacity at the third cycle. With the increasing of x, it can be easily found that the capacity will increase until x reaches 10% as highest point, and capacity decrease after that. If the coating is too thin or incomplete, it cannot fully protect the Li<sub>6</sub>PS<sub>5</sub>Cl from reacting with NMC 811, leading to the decomposition of the Li<sub>6</sub>PS<sub>5</sub>Cl electrolyte and the formation of side products at the interface. And the ion transfer would also be impeded by side products. As for a superfluous coating thickness, the ion transfer could be significantly restricted by the coating layer due to inadequate ionic conductivity of LiOH.

Fig. 5c shows the charge and discharge profiles of 10% LiOH-NMC 811 in the first three cycles at 0.126 mA cm<sup>-2</sup>. It delivers a high discharge specific capacity of 158.87 mAh g<sup>-1</sup> at the first discharge cycle, then 145.12 and 144.89 mAh g<sup>-1</sup> in the following cycles. The 10% LiOH-NMC 811 also demonstrated good rate performance, as shown in Fig. 5d. The battery was tested at various charge / discharge current densities from 0.1 to 1C with five cycles performed at each current density. The average reversible specific discharge capacities of 10% LiOH-NMC 811 are 159.3, 146.3, 130.5 and 119.4 mAh g<sup>-1</sup> at 0.1, 0.2, 0.5 and 1C, respectively. When the discharge current density went back to 0.1C at the end, the discharge capacity was almost recovered to the original value at the same rate for 161.9 mAh g<sup>-1</sup>, further demonstrating the excellent rate capability. The long-term cycling results of 10% LiOH-NMC 811 at 0.1C were shown in Fig. 5e. After about 100 cycles, the signal becomes noisy, this could be caused by temperature fluctuations during the test. The 10% LiOH-NMC 811 has an exceptional specific capacity of 130 mAh  $\rm g^{-1}$  on average with an ultra-stable 600 cycles with columbic efficiency of 98% and 90% capacity retention, verifying the excellent structural stability of 10% LiOH-NMC 811 cathode during the charge / discharge process.

Nonetheless, the LiOH–NMC 811 particles performed differently in the cells with liquid electrolyte. As shown in Fig. S3, an extra 5% LiOH sample gives the highest capacity for both cycle and rate tests. The capacity decreases significantly with an increased amount of LiOH. It is not surprising to see the difference. As for the NMC cathode applied in liquid electrolyte system, it takes great advantages of voids in the secondary NMC particles, which can increase the accessibility of the liquid electrolyte to the surface of NMC; however, this is not the case in the solid electrolyte system. [29] The presence of the LiOH layer blocked the immersion of liquid electrolyte into secondary particles of NMC 811 and the ion transfer between liquid electrolyte and cathode material is limited.

The cross-section elementary mapping results for electrode/electrolyte interfacial region before and after cycle were presented in Fig. S4. It is clear the as prepared electrode/electrolyte shows uniform and compact structure, Li<sub>6</sub>PS<sub>5</sub>Cl was homogeneously mixed with the LiOH–NMC 811 particles at cathode layer, with excellent aggregation at the interface with NMC, which will ensure the ion transfer. After the cycle test was finished, the ASSLB was disassembled, and the electrode/electrolyte interfacial area was mapped again for comparison. The structure of NMC particles did not change after cycling. Also, NMC particles were still fully wrapped in Li<sub>6</sub>PS<sub>5</sub>Cl structure without separation or cracking, further confirm the LiOH coating layer did not cause side reactions at the interface. The cycle performance also confirmed it.

A comparison among this work and serval recent researches on NMC coating, such as lithium niobium oxide coating via ALD on NMC 811 with PEO-based electrolyte (ALD-LNO-NMC 811), [30] lithium phosphate on NMC 811 by ALD (ALD-LPO), [31] Li-Ti-O coating on NMC 811 by solvothermal method (Solution-based LTO-NMC 811), [32] Tungsten Oxide Coating on NMC 811 with a sol-gel method (WO-NMC 811), [33] and chemical vapor deposition of polyaniline (PANI) nanoparticles on NMC 532 (CVD-PANI-NMC 532), [19] is graphed in Fig. 6. At the 200th cycle, the LiOH-NMC 811 in this work shows a capacity of 130 mAh g<sup>-1</sup> and 99.1% capacity retention. The capacity retention after 200 cycles was also greatly enhanced. The substantially improved electrochemical performance of 10% LiOH-NMC 811 so far largely comes from interface design, which successfully blocked the reaction between NMC and Li<sub>6</sub>PS<sub>5</sub>Cl, stabilized Li<sub>6</sub>PS<sub>5</sub>Cl to 4.0 V (vs Li / In) and optimized cathode ion diffusion. Compared to the previous research, the coating approach is much simpler and does not require extra step or equipment.

#### 4. Conclusion

In summary, we have developed a time- and cost-effective one-step sintering process to prepare LiOH coated NMC 811 material as the cathode for ASSLBs using Li<sub>6</sub>PS<sub>5</sub>Cl as solid electrolyte. Using a LiOH interfacial coating layer generated simultaneously during NMC 811 cathode sintering that only conducts ions but not electrons, the interface is secured due to the absence of electronic pathway for the sulfide electrolyte decomposition reaction. The 10 nm LiOH coating layer is able to stabilize the interface between the cathode and the Li<sub>6</sub>PS<sub>5</sub>Cl electrolyte so as to enhance the cyclability of the NMC 811 material, resulting in an outstanding coulombic efficiency (>99%), excellent cyclability (~130 mAh g-1 for 600 cycles) and satisfactory rate capability (119.4 mAh g<sup>-1</sup> at 1C). Furthermore, this strategy offers an alternative for stabilizing the cathode interface via a low-cost and scalable process that enables high-performance ASSLBs. It also provides an efficient strategy for developing advanced coating on other cathode materials for solid-state lithium-ion batteries, which can also be extended to other scalable high-performance electrochemical applications.

#### **Declaration of Competing Interest**

The authors declare no conflict of interest.

#### **CRediT authorship contribution statement**

Yubin Zhang: Conceptualization, Methodology, Formal analysis, Investigation, Resources, Writing - original draft. Xiao Sun: Conceptualization, Data curation, Formal analysis, Investigation, Methodology, Writing - review & editing. Daxian Cao: Formal analysis, Investigation, Writing - review & editing. Guanhui Gao: Formal analysis, Investigation. Zhenzhen Yang: Formal analysis, Investigation. Hongli Zhu: Conceptualization, Supervision, Writing - review & editing. Yan Wang: Conceptualization, Supervision, Writing - review & editing.

#### Acknowledgement

Y. W and Y. Z acknowledge the financial support by NSF DMR-1608398. H. Z acknowledge the financial support by NSF CBET-1924534.

#### Supplementary materials

Supplementary material associated with this article can be found, in the online version, at doi:10.1016/j.ensm.2021.06.024.

#### References

- D. Cao, et al., Processing strategies to improve cell-level energy density of metal sulfide electrolyte-based all-solid-state li metal batteries and beyond, ACS Energy Letters 5 (11) (2020) 3468–3489.
- [2] M.S. Whittingham, Lithium batteries and cathode materials, Chem. Rev. 104 (10) (2004) 4271–4301
- [3] MINING.COM. Available from: https://www.mining.com/markets/.
- [4] D. Mohanty, et al., Modification of Ni-rich FCG NMC and NCA cathodes by atomic layer deposition: preventing surface phase transitions for high-voltage lithium-ion batteries, Sci. Rep. 6 (2016) 26532.
- [5] R. Jung, et al., Oxygen release and its effect on the cycling stability of LiNixMnyCozO<sub>2</sub> (NMC) cathode materials for Li-ion batteries, J. Electrochem. Soc. 164 (7) (2017) A1361.
- [6] S.T. Myung, et al., Nickel-rich layered cathode materials for automotive lithium-ion batteries: achievements and perspectives, ACS Energy Letters 2 (1) (2017) 196–223.
- [7] B. Han, et al., Understanding the role of temperature and cathode composition on interface and bulk: optimizing aluminum oxide coatings for Li-ion cathodes, ACS Appl. Mater. Interfaces 9 (17) (2017) 14769–14778.
- [8] J.L. Shi, et al., High-capacity cathode material with high voltage for Li-ion batteries, Adv. Mater. 30 (9) (2018) 1705575.
- [9] J. Xu, et al., Understanding the degradation mechanism of lithium nickel oxide cathodes for Li-Ion batteries, ACS Appl. Mater. Interfaces 8 (46) (2016) 31677–31683.
- [10] J. Auvergniot, et al., Interface stability of argyrodite Li<sub>6</sub>PS<sub>5</sub>Cl toward LiCoO<sub>2</sub>, LiNi<sub>1</sub>/3Co1/3Mn1/3O<sub>2</sub>, and LiMn<sub>2</sub>O<sub>4</sub> in bulk all-solid-state batteries, Chem. Mater. 29 (9) (2017) 3883–3890.
- [11] D. Cao, et al., Stable thiophosphate-based all-solid-state lithium batteries through conformally interfacial nanocoating, Nano Lett. 20 (3) (2019) 1483–1490.
- [12] Z. Chen, et al., Role of surface coating on cathode materials for lithium-ion batteries, J. Mater. Chem. 20 (36) (2010) 7606–7612.
- [13] X. Song, M. Jia, R. Chen, Synthesis of Li<sub>3</sub>VO<sub>4</sub> by the citrate sol–gel method and its ionic conductivity, J. Mater. Process. Technol. 120 (1–3) (2002) 21–25.
- [14] B. Song, et al., Long-life nickel-rich layered oxide cathodes with a uniform Li<sub>2</sub>ZrO<sub>3</sub> surface coating for lithium-ion batteries, ACS Appl. Mater. Interfaces 9 (11) (2017) 9718–9725.
- [15] H. Kim, et al., A nano-LiNbO<sub>3</sub> coating layer and diffusion-induced surface control towards high-performance 5 V spinel cathodes for rechargeable batteries, J. Mater. Chem. A 5 (47) (2017) 25077–25089.
- [16] J. Xie, et al., Atomic layer deposition of stable LiAlF<sub>4</sub> lithium ion conductive interfacial layer for stable cathode cycling, ACS Nano 11 (7) (2017) 7019–7027.
- [17] M.R. Laskar, et al., Atomic layer deposition of Al<sub>2</sub>O<sub>3</sub>-Ga<sub>2</sub>O<sub>3</sub> alloy coatings for Li [Ni0. 5Mn0. 3Co0. 2] O2 cathode to improve rate performance in Li-Ion battery, ACS Appl. Mater. Interfaces 8 (16) (2016) 10572–10580.
- [18] J.Z. Kong, et al., Ultrathin ZnO coating for improved electrochemical performance of LiNi<sub>0.5</sub>Co<sub>0.2</sub>Mn<sub>0.3</sub>O<sub>2</sub> cathode material, J. Power Sources 266 (2014) 433–439.
- [19] M. Shao, et al., Selective adsorption-involved formation of NMC532/PANI microparticles with high ageing resistance and improved electrochemical performance, J. Energy Chem. 54 (2021) 668–679.
- [20] Y. Kim, H.S. Kim, S.W. Martin, Synthesis and electrochemical characteristics of Al2O3-coated LiNi1/3Co1/3Mn1/3O2 cathode materials for lithium ion batteries, Electrochim. Acta 52 (3) (2006) 1316–1322.
- [21] Y.P. Chen, et al., An approach to application for LiNi<sub>0.6</sub>Co<sub>0.2</sub>Mn<sub>0.2</sub>O<sub>2</sub> cathode material at high cutoff voltage by TiO2 coating, J Power Sources 256 (2014) 20–27.
- [22] B. Chen, et al., Systematic comparison of Al<sub>3</sub>+ Modified LiNi<sub>0.6</sub>Mn<sub>0.2</sub>Co<sub>0.2</sub>O<sub>2</sub> cathode material from recycling process, ACS Appl. Energy Mater. 2 (12) (2019) 8818–8825.
- [23] Z. Zheng, et al., High performance cathode recovery from different electric vehicle recycling streams, ACS Sustain Chem Eng 6 (11) (2018) 13977–13982.
- [24] J. Paulsen, J. Kim, High Nickel Cathode Material Having Low Soluble Base Content, Google Patents, 2017.
- [25] J.R. Ying, et al., Preparation and characterization of high-density spherical LiNi<sub>0.8</sub>Co<sub>0.2</sub>O<sub>2</sub> cathode material for lithium secondary batteries, J. Power Sources 99 (1–2) (2001) 78–84.
- [26] S. Deng, et al., Insight into cathode surface to boost the performance of solid-state batteries, Energy Storage Mater. 35 (2021) 661–668.
- [27] R. Jung, et al., Effect of ambient storage on the degradation of Ni-rich positive electrode materials (NMC811) for Li-ion batteries, J. Electrochem Soc. 165 (2) (2018) A132.
- [28] S.P. Culver, et al., On the functionality of coatings for cathode active materials in thiophosphate-based all-solid-state batteries, Adv. Energy Mater. 9 (24) (2019) 1900626.

- [29] Y. Mao, et al., High-voltage charging-induced strain, heterogeneity, and mi-Funct. Mater. 29 (18) (2019) 1900247.
- Funct. Mater. 29 (18) (2019) 1900247.
  [30] J. Liang, et al., Stabilizing and understanding the interface between nickel-rich cathode and PEO-based electrolyte by lithium niobium oxide coating for high-performance all-solid-state batteries, Nano Energy 78 (2020) 105107.
  [31] X.P. Cheng, et al., Realizing superior cycling stability of Ni-Rich layered cathode by combination of grain boundary engineering and surface coating, Nano Energy 62 (2019) 30–37.

- [32] Y.P. Huang, et al., Surface coating with Li-Ti-O to improve the electrochemical performance of Ni-rich cathode material, Appl. Surf. Sci. 489 (2019) 913–921.
   [33] D. Becker, et al., Surface modification of Ni-Rich LiNi<sub>0.8</sub>Co<sub>0.1</sub>Mn<sub>0.1</sub>O<sub>2</sub> cathode material by tungsten oxide coating for improved electrochemical performance in lithium-ion batteries, ACS Appl. Mater. Interfaces 11 (20) (2019) 18404–18414.